Journal of Clinical Monitoring and Computing (2019) 33:445–454
https://doi.org/10.1007/s10877-018-0169-5

ORIGINAL RESEARCH

Optimizing target control of the vessel rich group with volatile anesthetics

Christopher W. Connor[1,2]

Received: 9 March 2018 / Accepted: 7 June 2018 / Published online: 21 June 2018

Abstract
The ability to monitor the inspired and expired concentrations of volatile anesthetic gases in real time makes these drugs implicitly targetable. However, the end-tidal concentration only represents the concentration within the brain and the vessel rich group (VRG) at steady state, and very poorly approximates the VRG concentration during common dynamic situations such as initial uptake and emergence. How should the vaporization of anesthetic gases be controlled in order to optimally target VRG concentration in clinical practice? Using a generally accepted pharmacokinetic model of uptake and redistribution, a transfer function from the vaporizer setting to the VRG is established and transformed to the time domain. Targeted actuation of the vaporizer in a time-optimal manner is produced by a variable structure, sliding mode controller. Direct mathematical application of the controller produces rapid cycling at the limits of the vaporizer, further prolonged by low fresh gas flows. This phenomenon, known as "chattering", is unsuitable for operating real equipment. Using a simple and clinically intuitive modification to the targeting algorithm, a variable low-pass boundary layer is applied to the actuation, smoothing discontinuities in the control law and practically eliminating chatter without prolonging the time taken to reach the VRG target concentration by any clinically significant degree. A model is derived for optimum VRG-targeted control of anesthetic vaporizers. An alternate and further application is described, in which deliberate perturbation of the vaporization permits non-invasive estimation of parameters such as cardiac output that are otherwise difficult to measure intra-operatively.

Keywords Pharmacokinetics of anesthetic gases · Inhalational anesthesia · Control theory · System identification · Intraoperative monitoring · Anesthesia vaporizer design

1 Introduction

Volatile anesthetic agents continue to be the mainstay of contemporary anesthetic practice, though their pharmacokinetics set them apart from almost all other medications. The ability to monitor the inhaled and exhaled concentrations of volatile anesthetics makes these medications implicitly targetable [1]. Given sufficient time for equilibration to occur, the end-tidal agent concentration is held to represent the concentration in the vessel rich group (VRG), such that predictions about the patient's pharmacodynamic response can be made. This concept is foundational to the principle of minimum alveolar concentration (MAC) [2]. Consequently, targeting of the end-tidal agent concentration has been studied, either through control theory [3] or through engineering refinement of the anesthesia machine and circuit [4]. However it remains quite apparent, even in routine clinical practice, that the end-tidal agent concentration does not accurately reflect the effective concentration of the medication in the VRG during dynamic portions of anesthetic management such as either initial uptake or emergence. This focus on control based on targeting end-tidal agent concentration has neglected the more complex modulation necessary to target the true effective concentration in the VRG.

In essence, this problem is similar to that encountered during formalization of the mathematics required to perform target controlled infusion (TCI) of intravenous drugs. Models that target the plasma concentration are easier to derive, to solve, and to apply [5, 6]. However, during non-steady-state conditions, the plasma concentration and effect

✉ Christopher W. Connor
cconnor@bwh.harvard.edu

[1] Department of Anesthesiology, Perioperative and Pain Medicine, Brigham and Women's Hospital, 75 Francis Street, CWN L1, Boston, MA 02115, USA

[2] Department of Physiology and Biophysics, Boston University, Boston, MA, USA

concentration can diverge significantly. Therefore, modeling of the effect site concentration becomes necessary in order to produce a satisfactory TCI algorithm and an adequate pharmacodynamic response [7].

This report examines two hypotheses. Firstly, it is hypothesized that a control algorithm for targeting the volatile anesthetic concentration in the vessel rich group, based on control inputs applied to the anesthetic vaporizer, can be derived and characterized. An algorithm that is optimal in time is initially demonstrated, such that the vessel rich group concentration is brought to the desired target concentration in the shortest time interval after the command is given. Although this control algorithm is time-optimal, it may make mechanical demands upon the actuation of the vaporizer that could be practically limiting. Therefore, a second hypothesis is discussed and demonstrated: that a boundary-layer refinement of the control algorithm can produce comparably good time performance in targeting the VRG while avoiding rapid cycling at the limits of the controller. Alternative possible applications of the control algorithm are discussed, such as non-invasive intraoperative estimation of cardiac output.

2 Methods

This research report does not involve human subjects, either directly or indirectly via access to medical records and protected health information (PHI). Review by an Institutional Review Board (IRB) was not required.

Figure 1 illustrates a simplified compartmental model of the uptake and distribution of volatile anesthetic agents. The volatile model differs from the conventional mammillary model for intravenous agents [7] in that there is no central well-mixed compartment within the body into which drug is administered, and therefore distribution to deeper compartments is catenary and requires passage through intermediary compartments. The intravenous pharmacokinetic model is wholly abstract in its composition. In contrast, the volatile pharmacokinetic model retains physiologic features such as cardiac and respiratory circulations and recognizable tissue groups such as fat, muscle and the composite VRG. More complex models of respiratory uptake are available [8]; the model illustrated here neglects the relatively small effects of shunt and the vessel-poor group (VPG).

2.1 Pharmacokinetic modeling

The pharmacokinetic behavior of the model shown in Fig. 1 can be simulated using the set of simultaneous ordinary differential equations (Eqs. 1a–1g). As a simplifying assumption, both the arterial (ART) and venous (VEN) compartments are defined to come into equilibrium with the compartments through which they pass. The arterial concentration therefore reflects the alveolar concentration while neglecting shunt (Eq. 1c), and the venous concentration is an average of the concentrations of the deeper compartments weighted by their relative perfusion (Eq. 1g).

$$V_{ckt}\frac{dCKT}{dt} = \dot{V}_{fgf}(VAP - CKT) - \dot{V}_e(CKT - ALV) \quad (1a)$$

$$V_{alv}\frac{dALV}{dt} = \dot{V}_e(CKT - ALV) + Q\lambda_{blood}(VEN - ALV) \quad (1b)$$

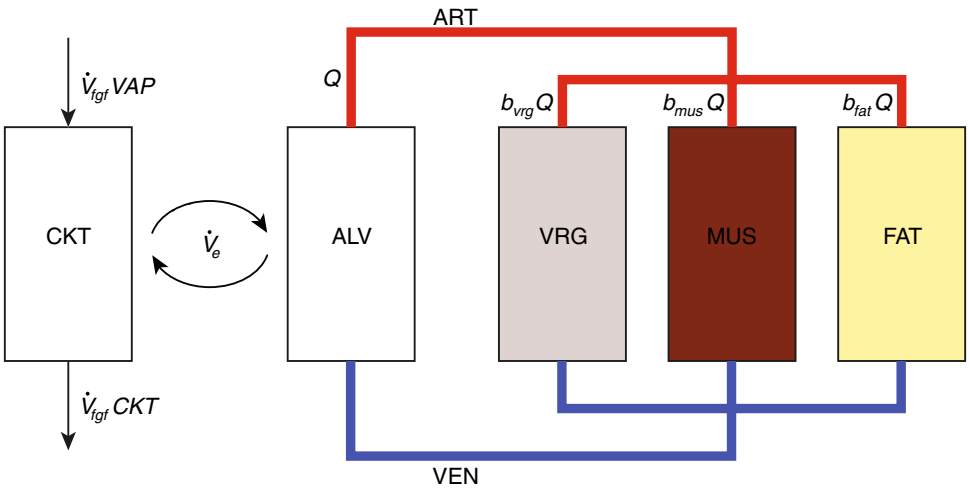

Fig. 1 Schematic representation of a compartmental pharmacokinetic model for the uptake and redistribution of volatile anesthetic gases, demonstrating the arrangement of the anesthesia machine circuit (CKT), alveoli (ALV), vessel rich group (VRG), muscle (MUS) and fat (FAT). Blood circulation is represented by the arterial (ART) and venous (VEN) compartments. Also shown are the vaporizer setting (VAP), fresh gas flow (V_{fgf}), minute ventilation (V_e), cardiac output (Q) and proportional distribution of blood flow to compartments (b_{vrg}, b_{mus}, b_{fat})

$$ART = ALV \tag{1c}$$

$$k_{vrg}\frac{dVRG}{dt} = ART - VRG \quad \text{where } k_{vrg}\frac{\lambda_{vrg}}{\lambda_{blood}} \cdot \frac{V_{vrg}}{b_{vrg}Q} \tag{1d}$$

$$k_{mus}\frac{dMUS}{dt} = ART - MUS \text{ where } k_{mus} = \frac{\lambda_{mus}}{\lambda_{blood}} \cdot \frac{V_{mus}}{b_{mus}Q} \tag{1e}$$

$$k_{fat}\frac{dFAT}{dt} = ART - FAT \quad \text{where } k_{fat} = \frac{\lambda_{fat}}{\lambda_{blood}} \cdot \frac{V_{fat}}{b_{fat}Q} \tag{1f}$$

$$VEN = b_{vrg}VRG + b_{mus}MUS + b_{fat}FAT \tag{1g}$$

Given a set of initial starting conditions (usually zero in all compartments), this system of differential equations can be numerically integrated forward to some future time in response to an arbitrary time course of inputs at the vaporizer (VAP, Eq. 1a) using standard Euler or Runge–Kutta techniques [9]. These time-domain models employ physiological parameters that are applicable to the clinical environment (such as fresh gas flow, minute ventilation), and use physicochemical solubility properties of the volatile agents (λ_{blood}, λ_{vrg}, λ_{muscle}, λ_{fat}) that are well characterized [10]. The utility of these models has been proven in both anesthesia education [11, 12] and guidance for clinical management [13, 14].

Numerical integration of the ordinary differential equations is satisfactory for determining the outcome of a known series of inputs, but it is not well suited to the inverse problem of determining the sequence of inputs required to produce a desired concentration in a targeted compartment such as the VRG. The design of such an algorithm begins by solving explicitly for the relationship between the concentration in the VRG and the vaporizer setting VAP. This can be achieved by taking the Laplace transform of the model system, such that the differential terms can be manipulated algebraically [15]. Transforming and substituting for ART and VEN (1g) produces a model in terms of the transforms of the five main compartments as shown in Eq. 2.

The model in Eq. 2 is a simultaneous equation of the form $A\underline{x} = \underline{n}$, where A is the matrix of coefficients, $\underline{x}$ is the transfer function for each compartment, and $\underline{n}$ is the system input. The equation system is linear with regard to the input, and therefore need only be solved for the simple step input $VAP = 1$; the output for any other time sequence of inputs can be obtained by repeated linear superposition of this solution. Additionally, it is useful to be able to incorporate any arbitrary initial concentrations in the compartments into the solution so that the control algorithm is able to proceed from any starting condition. The solution for the Vessel Rich Group is obtained by applying Cramer's rule using the determinants of the following matrices for a step input at the vaporizer A_{vap} (Eq. 3a) and arbitrary initial conditions A_{ini} (Eq. 3b) respectively.

$$A_{vap} = \begin{bmatrix} s + \frac{\dot{V}_e - \dot{V}_{fgf}}{V_{ckt}} & -\frac{\dot{V}_e}{V_{ckt}} & \frac{\dot{V}_{fgf}}{V_{ckt}} \cdot \frac{1}{s} & 0 & 0 \\ -\frac{\dot{V}_e}{V_{alv}} & s + \frac{\dot{V}_e + Q\lambda_{blood}}{V_{alv}} & 0 & -\frac{b_{mus}Q\lambda_{blood}}{V_{alv}} & -\frac{b_{fat}Q\lambda_{blood}}{V_{alv}} \\ 0 & -\frac{1}{k_{vrg}} & 0 & 0 & 0 \\ 0 & -\frac{1}{k_{mus}} & 0 & s + \frac{1}{k_{mus}} & 0 \\ 0 & -\frac{1}{k_{fat}} & 0 & 0 & s + \frac{1}{k_{fat}} \end{bmatrix} \tag{3a}$$

$$A_{ini} = \begin{bmatrix} s + \frac{\dot{V}_e - \dot{V}_{fgf}}{V_{ckt}} & -\frac{\dot{V}_e}{V_{ckt}} & CKT_0 & 0 & 0 \\ -\frac{\dot{V}_e}{V_{alv}} & s + \frac{\dot{V}_e + Q\lambda_{blood}}{V_{alv}} & ALV_0 & -\frac{b_{mus}Q\lambda_{blood}}{V_{alv}} & -\frac{b_{fat}Q\lambda_{blood}}{V_{alv}} \\ 0 & -\frac{1}{k_{vrg}} & VRG_0 & 0 & 0 \\ 0 & -\frac{1}{k_{mus}} & MUS_0 & s + \frac{1}{k_{mus}} & 0 \\ 0 & -\frac{1}{k_{fat}} & FAT_0 & 0 & s + \frac{1}{k_{fat}} \end{bmatrix} \tag{3b}$$

On applying Cramer's rule, as in Eq. 4a, a fraction is produced whose denominator is a fifth-order polynomial in the Laplace variable s. This polynomial is guaranteed to be real and to have only real roots [16]. A partial fraction expansion in terms of coefficients c and α is then performed, as described in "Appendix", and inversely transformed to the time domain as in Eq. 4b. The relationship between the

$$\begin{bmatrix} s + \frac{\dot{V}_e - \dot{V}_{fgf}}{V_{ckt}} & -\frac{\dot{V}_e}{V_{ckt}} & 0 & 0 & 0 \\ -\frac{\dot{V}_e}{V_{alv}} & s + \frac{\dot{V}_e + Q\lambda_{blood}}{V_{alv}} & -\frac{b_{vrg}Q\lambda_{blood}}{V_{alv}} & -\frac{b_{mus}Q\lambda_{blood}}{V_{alv}} & -\frac{b_{fat}Q\lambda_{blood}}{V_{alv}} \\ 0 & -\frac{1}{k_{vrg}} & s + \frac{1}{k_{vrg}} & 0 & 0 \\ 0 & -\frac{1}{k_{mus}} & 0 & s + \frac{1}{k_{mus}} & 0 \\ 0 & -\frac{1}{k_{fat}} & 0 & 0 & s + \frac{1}{k_{fat}} \end{bmatrix} \begin{bmatrix} \overline{CKT} \\ \overline{ALV} \\ \overline{VRG} \\ \overline{MUS} \\ \overline{FAT} \end{bmatrix} = \begin{bmatrix} \frac{\dot{V}_{fgf}}{V_{ckt}} \cdot \frac{VAP}{s} \\ 0 \\ 0 \\ 0 \\ 0 \end{bmatrix} \tag{2}$$

vaporizer setting VAP and the concentration in the VRG is therefore reduced to the summation of five weighted asymptotic exponential curves.

$$\overline{VRG} = \frac{VAP \cdot \left|A_{vap}\right|}{|A|} = VAP \cdot \left(\frac{c_1}{s+\alpha_1} + \frac{c_2}{s+\alpha_2} + \frac{c_3}{s+\alpha_3} + \frac{c_4}{s+\alpha_4} + \frac{c_5}{s+\alpha_5} \right) \tag{4a}$$

$$VRG(t) = VAP \cdot \left(c_1\left(e^{-\alpha_1 t} - 1\right) + c_2\left(e^{-\alpha_2 t} - 1\right) + c_3\left(e^{-\alpha_3 t} - 1\right) + c_4\left(e^{-\alpha_4 t} - 1\right) + c_5\left(e^{-\alpha_5 t} - 1\right) \right) \tag{4b}$$

2.2 Target control algorithm

The control algorithm for the VRG follows the form of a model predictive controller [17] using a discontinuous targeting algorithm as employed for effect site control of intravenous medications [7]. Specifically, the algorithm is a form of Sliding Mode Control (SMC) using a variable structure controller (VSC). The algorithm is applied every second, in the following stages:

1. The VRG concentration is projected forward assuming no input from the vaporizer (VAP = 0) for at least as many seconds as the peak one-second pulse response of the input. The 1-s pulse response is formed by the superposition of a 1% step response followed by a −1% step response delayed by one second, as illustrated in Fig. 2. The projection is not required to go beyond the peak of the pulse response, as the concentration in the VRG must necessarily be decreasing after that point for any previous combination of inputs.
2. If the target VRG concentration is exceeded, then the vaporizer input is set to zero for this interval.
3. The difference between the target concentration and the projection is divided point-wise by the pulse response. The minimum of this function is the vaporizer setting VAP that would bring the VRG concentration to the target without overshoot within the interval of the projection.
4. The vaporizer setting VAP calculated in step 3 is capped at the maximum permissible setting for the chosen agent (i.e., 5, 8 and 18% respectively for isoflurane, sevoflurane and desflurane).
5. A 1 s pulse of the volatile agent is applied at the input (i.e., the vaporizer) at the setting chosen.

2.3 Chattering

Chatter is a common, unwanted feature of variable structure, sliding-mode controllers, and exists due to the non-smooth transitions between the parts of the controller algorithm

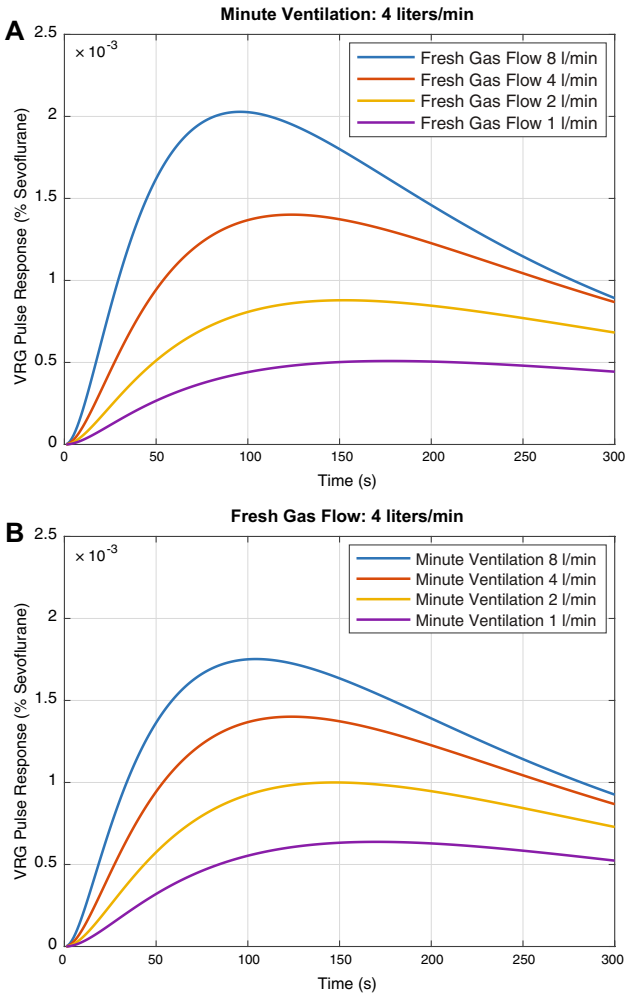

Fig. 2 Time-course of sevoflurane concentrations in the vessel rich group (VRG) in response to a one-second pulse of 1% sevoflurane at the vaporizer. **a** Variations in the pulse response with fresh gas flow while the minute ventilation is held constant at 4 l/min. **b** Variations in the pulse response with minute ventilation while the fresh gas flow is held constant at 4 l/min

[18]. In the target control algorithm for the VRG described above, the non-smooth transitions occur because of the hard upper and lower limits of actuation of the vaporizer. The controller may not exceed the maximum allowed vaporization for the agent in use, and a setting of less than 0% has no physical meaning. From a theoretical standpoint, there is no difficulty with a control algorithm that drives the control input between its saturation limits. For instance, to move a car at rest to another location at rest in the shortest time, one should accelerate as hard as possible and then break as hard as possible. This is the essence of "bang-bang" control [19], which has some particularly desirable properties such as rapidity of time response and a relative insensitivity to inaccuracies in the underlying system model. However, such rapidly-cycling control inputs run counter to human

preference and may be difficult to actuate upon real, physical equipment [17].

The customary approach to this problem is to create a "boundary layer", of which there are many theoretical designs [20], to smooth the transition between the regions of the control law when the target is approached to within some small distance, ε. For targeting the VRG, a boundary layer approach would imply that a new, smooth control law would cut in when the VRG concentration was within of $\pm\varepsilon$ the desired target. However, this approach only guarantees that the target will be approached within an error of ε, and is harder to implement when the target itself cannot be directly observed (as is the case here).

A modern, alternative solution is to use a form of low-pass filtering upon the input VAP [21]. An intuitively clinical approach is to replace the 1 s pulse in the controller algorithm with a longer duration pulse; i.e., the controller is required to choose the vaporization setting that it would select if the setting had to be maintained in that position for longer, while still choosing the setting that would bring the VRG to target in the shortest time without overshoot. For a pulse width w, the VRG response is given by $p_w(t)$ in Eq. 5. The responses shown in Fig. 2 are of the special case where $w=1$.

$$p_w(t) = \begin{cases} \sum_{i=1}^{5} c_i\left(e^{-\alpha_i t} - 1\right) & 0 \le t \le w \\ \sum_{i=1}^{5} c_i(e^{-\alpha_i w} - 1)e^{-\alpha_i(t-w)} & w < t \end{cases} \tag{5}$$

The control algorithm still operates every second, so the overall responsiveness of the algorithm is not compromised.

2.4 Statistical methods

Fitting of model parameters is performed using multivariate linear regression with least squares. The explanatory power is given in terms of the R^2 value, and the p value is calculated from the F statistic [22, 23].

3 Results

Figure 2 shows the time response of the concentration of volatile agent in the vessel rich group in response to a 1 s pulse of a setting of 1% at the sevoflurane vaporizer. Figure 2a shows a parametric variation in fresh gas flow, and Fig. 2b a parametric variation in minute ventilation. The response to any particular time course of inputs at the vaporizer can be constructed by summing appropriately linearly scaled and delayed response curves, i.e., by convolution. The increasingly sharp response curve with both fresh gas flow and minute ventilation demonstrate that both of these parameters favor increasing controllability of the VRG.

Figure 3 demonstrates the application of the target control algorithm to bring the VRG to a target concentration of 2% sevoflurane from an initially zero condition. Variations in fresh gas flow of 8, 4, 2 and 1 l/min are shown in Fig. 3a–d respectively. Increasing the fresh gas flow naturally decreases the time for the VRG to reach the target concentration, and in each case the control algorithm settles to a stable vaporizer setting (2.33, 2.44, 2.67 and 3.08% respectively for Fig. 3a–d). However, the behavior of the algorithm is notable for significant "chatter" in its actuation (VAP), in which the vaporizer setting is driven rapidly and alternatingly between its limits of 0 and 8%. This behavior is prolonged as the fresh gas flow is decreased. This is unfortunate as an algorithm that targets the VRG rather than end-tidal concentration would in general be of greatest use at lower fresh gas flows.

Figure 4 shows the effect of increasing the width of the low pass interval when applied to the controller response shown in Fig. 3b. The chattering is suppressed without increasing the time required to reach the VRG target concentration by any clinically significant amount.

Figure 5 shows a parametric study of agents, fresh gas flows, and cardiac outputs to determine the minimum width w of the low pass interval required such that only one rebound of greater than 0.1% is produced in the VAP input, as in Fig. 4d. A linear regression of the first three time constants of the VRG response closely predicts this value of w, with $R^2=0.956$ as shown in Table 1. A VRG target control algorithm is therefore demonstrated which offers time performance that is close to optimal while avoiding high-frequency inputs at the limits of the actuator.

4 Discussion

End-tidal control algorithms are available as implementations on current commercially-available anesthesia machines, although these features are not available in the US due to a lack of FDA approval. While the exact implementations of the commercial algorithms are proprietary, some details can be gleaned from the academic literature and from patent filings. Struys et al. [24] has an extensive appendix that describes many aspects of the Dräger Zeus, including the outline of its auto-control mode algorithm. This algorithm includes a parameter T_{delay} that models the response time of the hardware, i.e. the agent sensor and the vaporizer in combination. After first calculating a desired volume of agent to administer, the algorithm generates an average flow rate over the interval T_{delay}. Although the value of this interval is not given, this approach would be expected to suppress chatter in practice since it is analogous

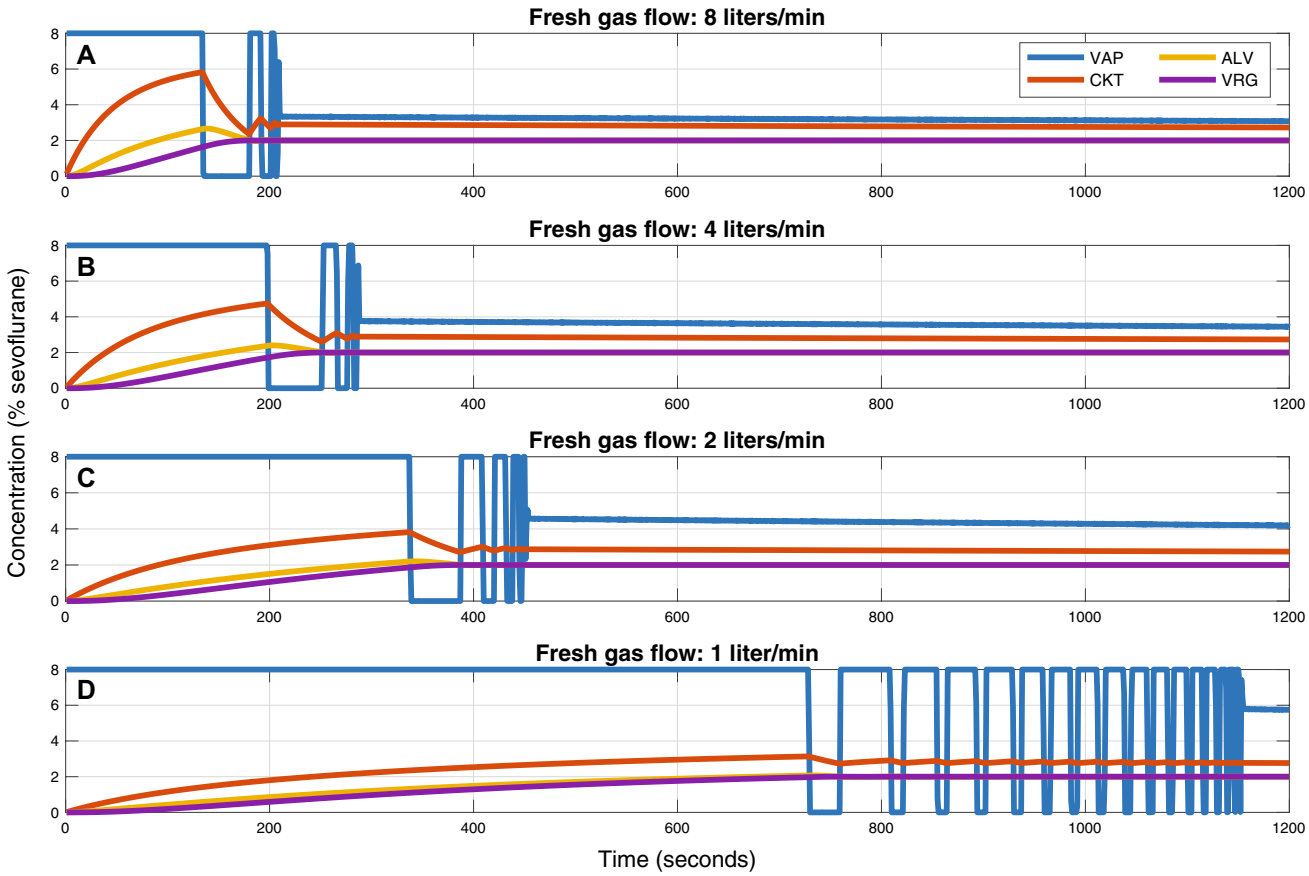

Fig. 3 Direct application of a sliding mode control algorithm produces accurate targeting of agent concentration within the vessel rich group (VRG) at the expense of significant chatter in the control input (VAP). The chatter is prolonged as fresh gas flow rates are reduced

to adopting a controller pulse width of $w = T_{delay}$ in Eq. 5. The Dräger algorithm is agnostic with regard to the effect site of the agent in the body: it instead seeks to bring the end-tidal concentration to the targeted value. The control law is described as a "traditional integral action controller", which is understood to mean a negative-feedback PI (proportional integral) controller. In the traditional PI controller, an error signal is first calculated, defined as the difference between the current output and the desired output. The controller input is then set as a multiple of the error signal (i.e., proportional), plus a multiple of the integration of the error signal over time (i.e., integral). The integral term gives the control law some "momentum" to reach the target: a purely proportional controller will only approach the target asymptotically but never reach it. A patent awarded to the General Electric Company, "Medical vaporizer and method of control of a medical vaporizer" [25], suggests that the GE platforms likely use a functionally similar mechanism of control.

The work described in this paper is, at this stage, a theoretical analysis in order to determine what the performance limits of VRG-guided control might be. The improvement inherent in the control algorithm described in this paper is that it explicitly targets the VRG pharmacokinetic compartment. Simply put, this allows the concentration in the VRG to be manipulated more quickly than end-tidal target control would permit. In order to raise the VRG quickly to a new target, a VRG-targeting control algorithm will initially push the end-tidal concentration above the target and then equilibrate. In order to lower the VRG concentration quickly, it will similarly take the end-tidal concentration below the new target for a period of time. In this way, the VRG-targeting algorithm mimics those actions that a skilled physician would naturally undertake in order to maximize control performance.

In the clinical setting, such a maximum-performance approach may not always be desired and the physician might choose to proceed more gradually. A similar issue exists with TCI algorithms—it is not always clinically desirable to use large boluses to bring the effect site concentration to the target in the shortest possible time. Van Pouke et al. [26] described a refinement of the standard TCI algorithm that limits peak plasma concentrations while still reaching the given effect site concentration in a reasonable time. A similar approach could be taken here.

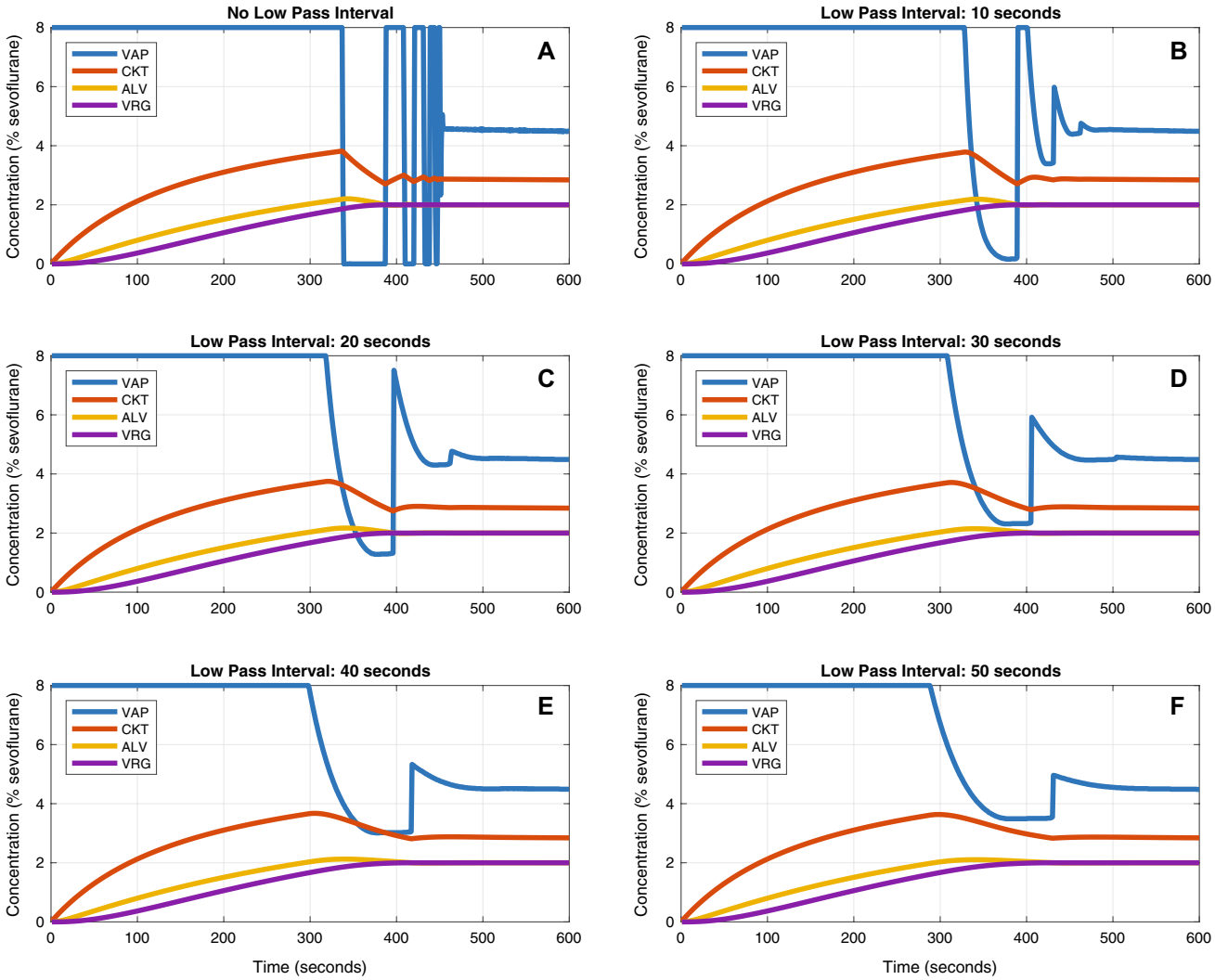

Fig. 4 Application of a variable low pass interval function to the sliding control mode algorithm almost completely eliminates chatter in the control input (VAP) without appreciably impairing the response time in the vessel rich group (VRG)

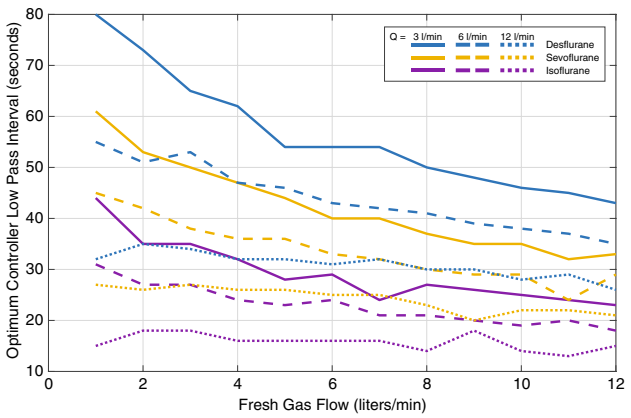

Fig. 5 The optimum widths of the controller algorithm low pass interval, as affected by choice of volatile agent, fresh gas flow and cardiac output. Minute ventilation is held constant at 4 l/min

Table 1 Linear regression model for the optimum controller low pass interval w (s)

	Coefficient estimate	Standard error	p value
$1/\alpha_1$ (s)	2.13	0.068	5.14×10^{-55}
$1/\alpha_2$ (s)	0.318	0.015	7.55×10^{-40}
$1/\alpha_3$ (s)	−0.037	0.003	1.36×10^{-24}
Intercept (s)	−7.81	0.97	1.53×10^{-12}

$w \approx \frac{2.13}{\alpha_1} + \frac{0.318}{\alpha_2} - \frac{0.037}{\alpha_3} - 7.81$ with $R^2 = 0.956$, $p = 1.63 \times 10^{-70}$

The shortest three time constants of the time-domain one-second pulse response are very strongly predictive of the optimum width of the controller low pass interval. An optimized controller produces accurate targeting of the vessel rich group concentration with minimized delay and input chatter

The algorithm is described using constant fresh gas flow (FGF) rates, but the consumption of volatile agents can be made more efficient by allowing the algorithm to reduce FGF as the desired VRG concentration is reached. This optimization is straightforward to implement. At each time step, the algorithm employs the lowest FGF that allows it to achieve the desired target within the simulation interval. If the target cannot be reached, it employs the highest FGF that it is allowed. If we set permissible lower and upper bounds for FGF at 0.3 and 12 l/min respectively, then the optimum FGF can be found using a bifurcating search. Suppose that the algorithm first tries an intermediate FGF of 6 l/min: it can use this intermediate result to refine the lower or upper bound accordingly. The algorithm will converge on the optimum FGF value in only a few steps.

The algorithm envisions the use of a plenum or variable-bypass type of vaporizer, but the algorithm can be generalized to direct liquid injection vaporizers. This is primarily achieved by relaxing the upper limit on the allowed vaporizer setting. As a rule of thumb, 1 ml of liquid anesthetic agent will typically produce approximately 200 ml of vapor. The exact value depends on the ambient temperature and pressure and on the liquid density and molecular weight of the agent used, according to the ideal gas equation $pV=nRT$. Suppose that an injection of 0.1 ml of agent is performed over 1 s to produce approximately 20 ml of vapor. If the fresh gas flow is 6 l/min (i.e., 100 ml/s) then the equivalent vaporization is approximately 20% for that 1 s.

With regard to the problem of chattering, as shown in Fig. 3, it is worth pointing out explicitly that this cannot be solved by the intuitively-appealing approach of increasing the rate at which the control algorithm performs adjustments (i.e., to increase the sampling rate, or bandwidth) in the hope that this might allow the algorithm to settle sooner. This approach would be incorrect. Increasing controller bandwidth can, paradoxically, worsen high-frequency controller behavior. The control behavior of the classic "fly-ball" governors of steam engines became *less* stable as the quality of their manufacturing was improved—a fact which perplexed engineers of the nineteenth century [27]. Speeding up the operation of the control algorithm would be unlikely to succeed because (i) the current algorithm period of 1 s is already an order of magnitude faster than the shortest time constant in Fig. 2, and (ii) lower fresh gas flows are associated with slower time constants, yet the chatter is worse in this setting.

An alternative application of this work involves keeping the VRG concentration within a set distance of a target while applying large variations to the vaporizer input in order to produce disturbances in the inspired and end-tidal concentration (ALV). These concentrations are directly measurable in the intraoperative setting by infrared spectroscopy. It is a mandated standard of care of the American Society of Anesthesiologists that there should be continual quantitative monitoring of end-tidal carbon dioxide during general anesthesia with an endotracheal tube [28]: all modern anesthesia machines also monitor inspired and expired anesthetic agent concentrations. By actively and carefully perturbing VAP under settings of known fresh gas flow and minute ventilation and observing changes in the CKT and ALV concentrations, it may be possible to discover useful clinical properties of the model (such as the cardiac output Q) in a non-invasive fashion. Some recent reviews of cardiac output monitoring do include techniques based upon respiratory gas kinetics [29, 30] and specifically describe its comparatively minimal invasiveness as a favorable characteristic [31] especially in patients whose airway is already controlled. A review by Funk *et al.* [32] provides numerous references for the estimation of cardiac output by having patients rebreathe their own expired CO_2, a method whose accuracy has more recently been reported to be improved by iterative refinements of the measurement [33]. The use of inert gases to measure cardiac output is established in adults [34], in children [35], and with use of volatile hydrocarbons as tracers [36]. Use of the patient's own expired CO_2 may have provided a regulatory advantage in that it does not require administration of an additional medication, but use of an explicit tracer gas may provide an advantage in terms of accuracy. Estimating cardiac output by careful manipulation of a volatile agent in a patient otherwise under anesthesia can perhaps satisfy both goals: no additional medication, but an explicit compound to trace nevertheless.

Using a similar analytical approach to that already described, and employing the common assumption that the end-tidal agent concentration is representative of the alveolar concentration, a model system for the end-tidal agent concentration (EtAg) can be written as in Eq. 6.

$$A_{etag} = \begin{bmatrix} s + \frac{\dot{V}_e - \dot{V}_{fgf}}{V_{ckt}} & \frac{\dot{V}_{fgf}}{V_{ckt}} \cdot \frac{1}{s} & 0 & 0 & 0 \\ -\frac{\dot{V}_e}{V_{alv}} & 0 & -\frac{b_{vrg} Q \lambda_{blood}}{V_{alv}} & -\frac{b_{mus} Q \lambda_{blood}}{V_{alv}} & -\frac{b_{fat} Q \lambda_{blood}}{V_{alv}} \\ 0 & 0 & s + \frac{1}{k_{vrg}} & 0 & 0 \\ 0 & 0 & 0 & s + \frac{1}{k_{mus}} & 0 \\ 0 & 0 & 0 & 0 & s + \frac{1}{k_{fat}} \end{bmatrix} \tag{6}$$

The inspired agent concentration can similarly be drawn from the circuit concentration. The results of Fig. 3 demonstrate that, with appropriate control, it may be possible to vary these inspired and expired agent concentrations aggressively while still restricting VRG concentration within close limits. This would produce a situation in which the patient's VRG concentration and hence depth of anesthesia would be approximately constant for clinical purposes, but in which both the inspired and end tidal concentrations could be perturbed, observed in real-time, and simultaneously predicted

from the state of the model. Kalman filtering [37] could then be used to optimally align the model state with the observed sequence of clinical values. An estimate of, for example, the current cardiac output Q could then be numerically extracted from the model state and displayed to the anesthesiologist. This possibility of real-time, intraoperative system discovery was originally suggested over 30 years ago [38], but it would have been wholly impractical on the hardware of the time, and the technique has never been introduced to clinical practice. However, digitally controlled vaporizers have since become relatively commonplace [39, 40] and enormous advances have been made in the availability of computing power. It may therefore now be feasible to implement these control algorithms on current anesthesia machines. An experimental approach might involve development with reference to PA catheters placed in pigs or sheep, followed by validation in humans with reference to transesophageal echocardiography.

Author contributions The manuscript is the sole work of the Corresponding Author.

Funding Funidng was provide by National Institute of General Medical Sciences (Grant No. NIH R01 GM121457-01A1), and also Departmental support.

Compliance with ethical standards

Conflict of interest Author declares that they have no conflict of interest.

Appendix: Source code for analytical solutions

The following MATLAB code (The MathWorks, Chestnut Hill, MA) performs the key analytical steps described in this paper.

```
% Physiological variables:
syms vckt vfgf ve valv QL kvrg kmus kfat bvrg bmus bfat

% Matrix representation of the simultaneous transfer functions.
syms s
A = [ s+(vfgf+ve)/vckt  -ve/vckt        0              0              0              ;
      -ve/valv          s+(ve+QL)/valv  -QL*bvrg/valv  -QL*bmus/valv  -QL*bfat/valv ;
      0                 -1/kvrg         s+1/kvrg       0              0              ;
      0                 -1/kmus         0              s+1/kmus       0              ;
      0                 -1/kfat         0              0              s+1/kfat       ];

% Solve for the analytical solution for the vessel rich group in response
% to a step input at the vaporizer, using Cramer's rule.
% The solution is then expressed as the partial fraction expansion:
% VRG(s) = c1/(s+a1) + c2/(s+a2) + c3/(s+a3) + c4/(s+a4) + c5/(s+a5)
syms a1 a2 a3 a4 a5
syms c1 c2 c3 c4 c5
n = [(vfgf/vckt)*(1/s) ; 0 ; 0 ; 0 ; 0];
Avap = [A(:,1:2) n A(:,4:5)];
PFE = (s+a1)*(s+a2)*(s+a3)*(s+a4)*(s+a5);
c1 = simplify(subs((s+a1)*det(Avap)/PFE,s,-a1));
c2 = simplify(subs((s+a2)*det(Avap)/PFE,s,-a2));
c3 = simplify(subs((s+a3)*det(Avap)/PFE,s,-a3));
c4 = simplify(subs((s+a4)*det(Avap)/PFE,s,-a4));
c5 = simplify(subs((s+a5)*det(Avap)/PFE,s,-a5));

% After the symbolic manipulation is done, the physiological variables can
% be replaced by their numerical values. Numerical values for a and c terms
% can then be generated as follows:
factors = -roots(eval(fliplr(coeffs(det(A),s))));
a1 = factors(1); a2 = factors(2); a3=factors(3); a4=factors(4); a5=factors(5);
c1 = eval(c1); c2 = eval(c2); c3 = eval(c3); c4 = eval(c4); c5 = eval(c5);
```

References

1. Gupta DK, Eger EI. Inhaled anesthesia: the original closed-loop drug administration paradigm. Clin Pharmacol Ther. 2008;84(1):15–8.
2. Eger EI, Saidman LJ, Brandstater B. Minimum alveolar anesthetic concentration: a standard of anesthetic potency. Anesthesiology. 1965;26(6):756–63.
3. Sieber TJ, Frei CW, Derighetti M, Feigenwinter P, Leibundgut D, Zbinden AM. Model-based automatic feedback control versus human control of end-tidal isoflurane concentration using low-flow anaesthesia. Br J Anaesth. 2000;85(6):818–25.
4. Lortat-Jacob B, Billard V, Buschke W, Servin F. Assessing the clinical or pharmaco-economical benefit of target controlled desflurane delivery in surgical patients using the Zeus anaesthesia machine. Anaesthesia. 2009;64(11):1229–35.
5. Shafer SL, Siegel LC, Cooke JE, Scott JC. Testing computer-controlled infusion pumps by simulation. Anesthesiology. 1988;68(2):261–6.
6. Bailey JM, Shafer SL. A simple analytical solution to the three-compartment pharmacokinetic model suitable for computer-controlled infusion pumps. IEEE Trans Biomed Eng. 1991;38(6):522–5.
7. Shafer SL, Gregg KM. Algorithms to rapidly achieve and maintain stable drug concentrations at the site of drug effect with a computer-controlled infusion pump. J Pharmacokinet Biopharm. 1992;20(2):147–69.
8. Zwart A, Seagrave RC, Van Dieren A. Ventilation-perfusion ratio obtained by a noninvasive frequency response technique. J Appl Physiol. 1976;41(3):419–24.
9. Ascher UM, Petzold LR. Computer methods for ordinary differential equations and differential-algebraic equations. Philadelphia: Society for Industrial and Applied Mathematics; 1998.
10. Yasuda N, Targ AG, Eger EI. Solubility of I-653, sevoflurane, isoflurane, and halothane in human tissues. Anesth Analg. 1989;69(3):370–3.
11. Heffernan PB, Gibbs JM, McKinnon AE. Teaching the uptake and distribution of halothane. A computer simulation program. Anaesthesia. 1982;37(1):9–17.
12. Garfield JM, Paskin S, Philip JH. An evaluation of the effectiveness of a computer simulation of anaesthetic uptake and distribution as a teaching tool. Med Educ. 1989;23(5):457–62.
13. Kennedy RR, French RA, Gilles S. The effect of a model-based predictive display on the control of end-tidal sevoflurane concentrations during low-flow anesthesia. Anesth Analg. 2004;99(4):1159–63.
14. Kuo AS, Vijjeswarapu MA, Philip JH. Incomplete spontaneous recovery from airway obstruction during inhaled anesthesia induction: a computational simulation. Anesth Analg. 2016;122(3):698–705.
15. Stroud KA. Laplace transforms: programmes and problems. New York: Wiley; 1973. ISBN 0470834153.
16. Jenkins M, Traub JF. A three-stage algorithm for real polynomials using quadratic iteration. SIAM J Num Anal. 1970;7(4):545–66.
17. Garcia CE, Prett DM, Morari M. Model predictive control: theory and practice—a survey. Automatica. 1989;25(3):335–48.
18. DeCarlo RAZ, Drakunov SH, S.V. Variable Structure, Sliding-Mode Controller Design. In: Levine WS, The Control Handbook. New York, NY: IEEE Press; 1996.
19. Sonneborn L, Van Vleck F. The bang-bang principle for linear control systems. J Soc Ind Appl Math A. 1964;2(2):151–9.
20. Hung JY, Gao W, Hung JC. Variable structure control: a survey. IEEE Trans Industr Electron. 1993;40(1):2–22.
21. Tseng ML, Chen MS. Chattering reduction of sliding mode control by low-pass filtering the control signal. Asian Journal of Control. 2010;12(3):392–8.
22. Draper NR, Smith H. Applied regression analysis. Wiley series in probability and mathematical statistics. 2d ed. New York: Wiley; 1981.
23. Chatterjee S, Hadi AS. (1986) Influential observations, high leverage points, and outliers in linear regression. Stat Sci. 1:379–93.
24. Struys MM, Kalmar AF, De Baerdemaeker LE, Mortier EP, Rolly G, Manigel J, Buschke W. Time course of inhaled anaesthetic drug delivery using a new multifunctional closed-circuit anaesthesia ventilator. In vitro comparison with a classical anaesthesia machine. Br J Anaesth. 2005;94(3):306–17.
25. Bottom DK. (2013) Medical vaporizer and method of control of a medical vaporizer. US Patent and Trademark Office, US8752544.
26. Van Poucke GE, Bravo LJ, Shafer SL. Target controlled infusions: targeting the effect site while limiting peak plasma concentration. IEEE Trans Biomed Eng. 2004;51(11):1869–75.
27. Kang C-G. Origin of Stability Analysis: "On Governors" by JC Maxwell. IEEE Control Systems. 2016;36(5):77–88.
28. Standards for Basic Anesthetic Monitoring. Committee of Origin: Standards and Practice Parameters (2016). Approved by the ASA House of Delegates on October 21, 1986, last amended on October 20, 2010, and last affirmed on October 28, 2016. edn. American Society of Anesthesiologists, http://www.asahq.org/~/media/Sites/ASAHQ/Files/Public/Resources/standards-guidelines/standards-for-basic-anesthetic-monitoring.pdf.
29. Sangkum L, Liu GL, Yu L, Yan H, Kaye AD, Liu H. Minimally invasive or noninvasive cardiac output measurement: an update. J Anesth. 2016;30(3):461–80.
30. Thiele RH, Bartels K, Gan TJ. Cardiac output monitoring: a contemporary assessment and review. Crit Care Med. 2015;43(1):177–85.
31. Drummond KE, Murphy E. Minimally invasive cardiac output monitors. Cont Educ Anaesth Crit Care Pain. 2011;12(1):5–10.
32. Funk DJ, Moretti EW, Gan TJ. Minimally invasive cardiac output monitoring in the perioperative setting. Anesth Analg. 2009;108(3):887–97.
33. Klein M, Minkovich L, Machina M, Selzner M, Spetzler VN, Knaak JM, Roy D, Duffin J, Fisher JA. Non-invasive measurement of cardiac output using an iterative, respiration-based method. Br J Anaesth. 2015;114(3):406–13.
34. Agostoni P, Cattadori G. Noninvasive cardiac output measurement: a new tool in heart failure. Cardiology. 2009;114(4):244–6.
35. Wiegand G, Kerst G, Baden W, Hofbeck M. Noninvasive cardiac output determination for children by the inert gas-rebreathing method. Pediatr Cardiol. 2010;31(8):1214–8.
36. Bogaard HJ, Wagner PD. Measurement of cardiac output by open-circuit acetylene uptake: a computer model to quantify error caused by ventilation-perfusion inequality. Physiol Meas. 2006;27(10):1023–32.
37. Kalman RE. A new approach to linear filtering and prediction problems. J Basic Eng. 1960;82(1):35–45.
38. Akman G, Kaufman H, Roy R. Continuous pulmonary capillary blood flow estimation from measurements of respiratory anesthetic gas concentration. IEEE Trans Bio-Med Eng. 1985;32(12):1017–31.
39. Hendrickx JF, De Cooman S, Deloof T, Vandeput D, Coddens J, De Wolf AM. The ADU vaporizing unit: a new vaporizer. Anesth Analg. 2001;93(2):391–5.
40. Young J, Kapoor V. Principles of anaesthetic vaporizers. Anaesth Intens Care Med. 2013;14(3):99–102.